



ARL-TR-8200 • Nov 2017



# Dilution of Precision as a Geometry Metric for Swarm Relative Localization

by Michael L Don

Approved for public release; distribution is unlimited.

## **NOTICES**

### **Disclaimers**

The findings in this report are not to be construed as an official Department of the Army position unless so designated by other authorized documents.

Citation of manufacturer's or trade names does not constitute an official endorsement or approval of the use thereof.

Destroy this report when it is no longer needed. Do not return it to the originator.



# **Dilution of Precision as a Geometry Metric for Swarm Relative Localization**

**by Michael L Don**

*Weapons and Materials Research Directorate, ARL*

**REPORT DOCUMENTATION PAGE**

*Form Approved  
OMB No. 0704-0188*

Public reporting burden for this collection of information is estimated to average 1 hour per response, including the time for reviewing instructions, searching existing data sources, gathering and maintaining the data needed, and completing and reviewing the collection information. Send comments regarding this burden estimate or any other aspect of this collection of information, including suggestions for reducing the burden, to Department of Defense, Washington Headquarters Services, Directorate for Information Operations and Reports (0704-0188), 1215 Jefferson Davis Highway, Suite 1204, Arlington, VA 22202-4302. Respondents should be aware that notwithstanding any other provision of law, no person shall be subject to any penalty for failing to comply with a collection of information if it does not display a currently valid OMB control number.

**PLEASE DO NOT RETURN YOUR FORM TO THE ABOVE ADDRESS.**

<b>1. REPORT DATE (DD-MM-YYYY)</b> November 2017			<b>2. REPORT TYPE</b> Technical Report		<b>3. DATES COVERED (From - To)</b> August 2017	
<b>4. TITLE AND SUBTITLE</b> Dilution of Precision as a Geometry Metric for Swarm Relative Localization					<b>5a. CONTRACT NUMBER</b>	
					<b>5b. GRANT NUMBER</b>	
					<b>5c. PROGRAM ELEMENT NUMBER</b>	
<b>6. AUTHOR(S)</b> Michael L Don					<b>5d. PROJECT NUMBER</b>	
					<b>5e. TASK NUMBER</b>	
					<b>5f. WORK UNIT NUMBER</b>	
<b>7. PERFORMING ORGANIZATION NAME(S) AND ADDRESS(ES)</b> US Army Research Laboratory ATTN: RDRL-WML-F Aberdeen Proving Ground, MD 21005-5066					<b>8. PERFORMING ORGANIZATION REPORT NUMBER</b>  ARL-TR-8200	
<b>9. SPONSORING/MONITORING AGENCY NAME(S) AND ADDRESS(ES)</b>					<b>10. SPONSOR/MONITOR'S ACRONYM(S)</b>	
					<b>11. SPONSOR/MONITOR'S REPORT NUMBER(S)</b>	
<b>12. DISTRIBUTION/AVAILABILITY STATEMENT</b> Approved for public release; distribution is unlimited.						
<b>13. SUPPLEMENTARY NOTES</b>						
<b>14. ABSTRACT</b> Swarms of agents can use range measurements to achieve relative localization. The accuracy of this localization is affected by the geometry of the swarm agents. To characterize the swarm geometry, a metric is needed that relates the geometry to localization accuracy. Such a metric, called Dilution of Precision (DOP), is commonly used for global positioning systems (GPSs). GPS differs from swarm relative localization, however, in that there is an unknown receiver clock bias, the localization is absolute instead of relative, and all of the satellite positions are known. This report derives a DOP metric suitable for swarm relative localization and investigates its utility in several example cases.						
<b>15. SUBJECT TERMS</b> dilution of precision, DOP, localization, GPS, swarm, time-of-flight ranging, TOF, two-way ranging, TWR						
<b>16. SECURITY CLASSIFICATION OF:</b>			<b>17. LIMITATION OF ABSTRACT</b>  UU	<b>18. NUMBER OF PAGES</b>  34	<b>19a. NAME OF RESPONSIBLE PERSON</b> Michael L Don	
<b>a. REPORT</b> Unclassified	<b>b. ABSTRACT</b> Unclassified	<b>c. THIS PAGE</b> Unclassified			<b>19b. TELEPHONE NUMBER (Include area code)</b> 410-306-0775	

## Contents

---

---

<b>List of Figures</b>	<b>iv</b>
<b>List of Tables</b>	<b>v</b>
<b>Acknowledgments</b>	<b>vi</b>
<b>1. Introduction</b>	<b>1</b>
<b>2. GPS Localization and DOP</b>	<b>2</b>
2.1 GPS Localization	2
2.2 Intuitive DOP Illustration	4
2.2 GPS DOP	5
2.3 Comparison of GPS DOP to Root-Mean-Square Error	7
<b>3. TWR Localization and DOP with Anchors</b>	<b>8</b>
3.1 TWR Localization and DOP Derivation	8
3.2 Comparison of TWR DOP and RMSE Using Anchors	9
<b>4. Swarm Relative Localization and DOP</b>	<b>12</b>
4.1 Swarm Relative Localization	12
4.2 Comparison of Average TWR DOP to RMSE	13
4.2.1 Increasing DOP Example	13
4.2.2 Constant DOP Example	16
4.2.3 Example of Inconsistent DOP and RMSE Values	18
4.3 A Simple Application for Swarm Relative Localization DOP	20
<b>5. Conclusion</b>	<b>21</b>
<b>6. References</b>	<b>23</b>
<b>List of Symbols, Abbreviations, and Acronyms</b>	<b>24</b>
<b>Distribution List</b>	<b>25</b>

## List of Figures

---

Fig. 1	Agent location estimation from noisy TOF range measurements using Gauss–Newton algorithm.....	4
Fig. 2	Example of geometry with low DOP (left) and high DOP (right).....	5
Fig. 3	An example geometry with a low PDOP (left) and a high PDOP (right) .....	6
Fig. 4	Agent location estimation from noisy TOF range measurements for 6 different agent locations.....	7
Fig. 5	Comparison of DOP and RMSE values for the simulation in Fig. 4....	8
Fig. 6	Agent location estimation from noisy TWR measurements using Gauss–Newton algorithm.....	10
Fig. 7	Agent location estimation from noisy TWR measurements for 6 agent locations .....	11
Fig. 8	Comparison of DOP and RMSE values for the simulation in Fig. 7..	11
Fig. 9	Initial agent locations for swarm DOP simulation.....	14
Fig. 10	Thirty-one different swarm positions generated from Fig. 9 by scaling all of the $\mathbf{x}$ coordinates of the agents and some of the $\mathbf{z}$ coordinates .	14
Fig. 11	Estimated swarm position from noisy measurements for 6 of the swarms shown in Fig. 10 .....	15
Fig. 12	RMSE error and average DOP results for the simulation in Fig. 11 ..	16
Fig. 13	Estimated swarm position from noisy measurements for 6 swarms with all components of the agent’s positions linearly scaled.....	17
Fig. 14	RMSE error and average DOP results for the simulation in Fig. 13 ..	17
Fig. 15	Estimated swarm position from noisy measurements for 6 swarms with only one agent’s position scaled .....	18
Fig. 16	RMSE error and average DOP results for the simulation in Fig. 15 ..	18
Fig. 17	Results of Kabsch algorithm after noise was added directly to the position of agent 8, with the scale factor set to 1 .....	19
Fig. 18	Results of Kabsch algorithm after noise was added directly to the position of agent 8, with the scale factor set to 10.....	20
Fig. 19	A comparison of the RMSE of the scaled agent to the average of the other agents .....	20
Fig. 20	Four cases of swarm relative localization with different swarm sizes. The upper left has 6 agents, the upper right 8, lower left 12, and the lower right 20 agents.....	21

## List of Tables

---

---

Table 1	GPS DOP values for Fig. 3 .....	7
Table 2	TWR DOP values for Fig. 3 .....	9
Table 3	PDOP and RMSE values for different swarm sizes.....	21

## **Acknowledgments**

---

I would like to thank Moshe Hamaoui of the US Army Research Laboratory for his editing and suggestions.

## 1. Introduction

---

Swarms of cooperating agents exhibit advantages over a comparable group of solitary individuals. One advantage is the ability for swarm agents to localize relative to the group, using spatial relationships among many agents to achieve accurate relative position information.<sup>1</sup> This is particularly important in global positioning system (GPS)-denied environments where there are limited options for positioning.<sup>2</sup> Swarm relative localization has many applications, such as location-aware networking protocols,<sup>3</sup> collision avoidance,<sup>4</sup> formation flying,<sup>5</sup> and patterned weapon delivery.<sup>6</sup>

One method to achieve swarm localization is through estimating agent positions from noisy range measurements between agents. A key design parameter in such a localization scheme is the agents' estimated position accuracy. This accuracy is not solely based on the quality of the range measurements. Swarm geometry plays an important role in localization error.<sup>7</sup> The relationship between the agent's geometry and localization error is called dilution of precision (DOP) and is commonly used in GPS error characterization. The GPS satellite constellations were carefully constructed to limit the amount of DOP experienced by GPS receivers. A similar DOP metric to relate swarm geometry to localization error is needed for swarm system design and error prediction.

Although the GPS DOP metric is a good starting point when considering a swarm DOP metric, GPS DOP cannot be directly applied to swarm localization for 3 reasons. First, GPS uses time-of-flight (TOF) ranging, which requires the receiver's clock bias to be factored into the DOP measurements. Typical swarm range measurements use two-way ranging (TWR), which is independent of clock bias.<sup>8</sup> Second, GPS satellites have known absolute positions that are used to determine the receiver's location. Thus, a single DOP value characterizes the quality of satellites' geometry with respect to the receiver. In swarm relative localization, all of the agents' positions are unknown, and their locations must be solved collectively, forcing us to consider the geometry of the swarm with respect to each agent. Third, since the absolute positions of the satellites are known, the absolute position of the receiver can also be found. This makes measuring the receiver's position error straightforward. In contrast, localization of a swarm is relative, with no absolute position with which to measure precision. As we will see, this can make the relationship between DOP and position error problematic.

Before developing a DOP for relative swarm localization, the general concept of DOP will be presented, followed by an explanation of GPS localization and DOP. GPS is an example of localization using TOF ranging with anchors. As the first step in developing a DOP metric for swarms, TWR localization and DOP with anchors will be derived. This DOP metric will then be applied to swarm relative localization without anchors, and its utility will be analyzed through a few example cases. Finally, a simple example application of DOP relating to swarm system design will be demonstrated.

## 2. GPS Localization and DOP

---

### 2.1 GPS Localization

---

GPS uses TOF ranging between satellites at known positions and the GPS receiver. To generalize, the satellites and receiver will be referred to as the anchors and agent, respectively. The GPS range equation is<sup>9</sup>

$$p' = d + c(dt_x - dt_a) + d_{ion} + d_{trop} + e', \quad (1)$$

where  $d$  is the distance from the agent to the anchor,  $dt_x$  and  $dt_a$  are the clock offsets of the agent and anchors, respectively,  $d_{ion}$  and  $d_{trop}$  are the distance biases due to the ionosphere and troposphere,  $e'$  is the noise error, and  $p'$  is the uncorrected pseudorange. The term pseudorange is used because of the additional distances included in  $p'$  aside from the actual range measurement. Taking into account  $dt_a$ ,  $d_{ion}$ , and  $d_{trop}$  corrections made by the GPS model, the corrected pseudorange is

$$p = d + c(dt_x) + e, \quad (2)$$

leaving only agent's clock offset  $c(dt_x)$  as an additional distance to the geometric range. The error for the corrected pseudorange,  $e$ , now also includes the modeling errors of the corrected terms. Given  $n$  anchors with positions  $\mathbf{a}_i \in \mathbb{R}^3$  for  $1 \leq i \leq n$ , one agent at estimated position  $\mathbf{x} \in \mathbb{R}^4$ , where  $x_i$  for  $1 \leq i \leq 3$  is the agent position and  $x_4$  is a measurement offset due to clock bias, the  $n$  pseudoranges between the anchors and agent are

$$p_i = \|\mathbf{x}' - \mathbf{a}_i\| + x_4 + e_i, \quad (3)$$

where  $\|\cdot\|$  represents the Euclidean norm and  $\mathbf{x}' = \{x_1, x_2, x_3\}$ . Using Eq. 3, the agent's position can be found from pseudorange measurements through a least-squares iterative method such as the Gauss–Newton algorithm.<sup>10</sup> The algorithm begins by defining  $n$  residuals as

$$r_i = \|\mathbf{x}' - \mathbf{a}_i\| + x_4 - p_i, \quad (4)$$

where  $p_i$  now represents the measured pseudorange from the anchor to the agent, and  $\mathbf{x}$  contains the unknown agent position and offset. Thus, the residuals are simply the differences between the estimated pseudoranges and measured pseudoranges.  $\mathbf{x}$  is found by minimizing the sum of squares of the residuals:

$$S(\mathbf{x}) = \sum_{i=1}^n r_i^2(\mathbf{x}). \quad (5)$$

The algorithm progresses in iterations of

$$\mathbf{x}^{(k+1)} = \mathbf{x}^{(k)} - (\mathbf{J}^T \mathbf{J})^{-1} \mathbf{J}^T \mathbf{r}(\mathbf{x}^{(k)}) \quad (6)$$

using  $\mathbf{x}^{(0)}$  as an initial guess of the agent's position and offset, and Jacobian matrix  $\mathbf{J} \in \mathbb{R}^{n \times 4}$  with entries

$$J_{ij} = \frac{\partial r_i(\mathbf{x})}{\partial x_j}. \quad (7)$$

Expanding  $r_i$  gives

$$J_{ij} = \frac{\partial}{\partial x_j} \left[ ((x_1 - a_{i1})^2 + (x_2 - a_{i2})^2 + (x_3 - a_{i3})^2)^{\frac{1}{2}} + x_4 - p_i \right]. \quad (8)$$

For  $1 \leq j \leq 3$ ,  $\frac{\partial p_i}{\partial x_j} = \frac{\partial x_4}{\partial x_j} = 0$ , so that we have

$$J_{ij} = \left( \frac{1}{2} \right) ((x_1 - a_{i1})^2 + (x_2 - a_{i2})^2 + (x_3 - a_{i3})^2)^{-\frac{1}{2}} (2x_j). \quad (9)$$

For  $j = 4$ ,  $J_{ij} = 1$ . After simplifying, matrix  $\mathbf{J}$  has elements

$$J_{ij} = \begin{cases} \frac{x_j - a_{ij}}{\|\mathbf{x} - \mathbf{a}_i\|}, & 0 \leq j \leq 3 \\ 1, & j = 4 \end{cases} \quad (10)$$

Figure 1 shows a simulation of GPS localization with anchors positioned on the vertices of a unit cube and the agent in the center, with distances left unitless in this report. Ten sets of range measurements were simulated with Gaussian noise with standard deviation  $\sigma = 0.25$  and offset  $c(dt_x) = 0.5$ , resulting in 10 estimated agent positions marked by blue "X's". The cube anchor geometry offers a convenient symmetric geometry, even though the occlusion of the satellites by the earth would make this configuration impossible in reality.

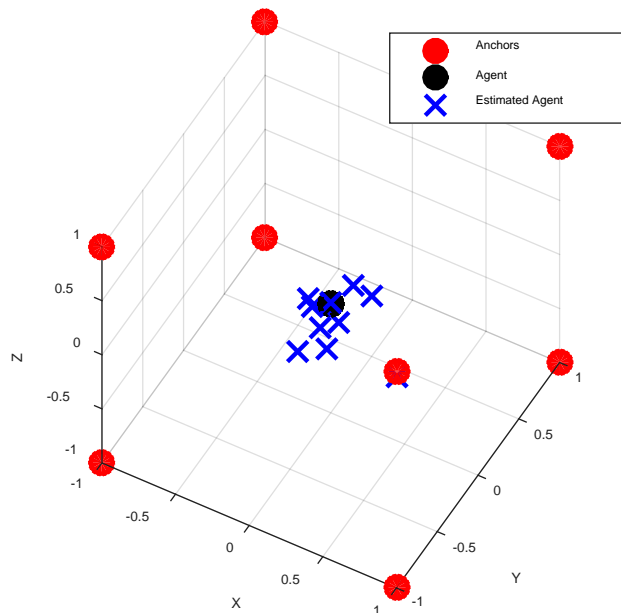


**Fig.1 Agent location estimation from noisy TOF range measurements using Gauss–Newton algorithm**

## 2.2 Intuitive DOP Illustration

Before proceeding with a quantitative definition of DOP, an intuitive example will be given to illustrate the basic concept. Figure 2 shows 2 example localization geometries. The anchors are shown as red circles, and the agent is shown as a small black circle. A range measurement from an anchor to the agent, denoted as  $d$ , limits the possible positions of the agent in 2 dimensions to a circle around the anchor with radius  $d$ . With the addition of measurement noise, this circle transforms into a region where the red circles designate an upper bound on the true range and the green circles designate a lower bound. The area where these regions overlap is colored blue and bounds the possible location of the agent. In the example on the left, the 3 anchors are spread out, creating a small region of uncertainty for the agent, indicating a small DOP. On the right, the anchors are close together, resulting in a larger region of uncertainty, indicating a large DOP. Additionally, DOP values can be calculated for separate position components. The example on the right has a large uncertainty in the  $y$  direction but is relatively narrow in the  $x$  direction. This can be characterized by using different DOP values for  $x$  and  $y$ . This example did not take into account any time dilution as exists in GPS applications, but the general idea remains the same. The hard boundaries of the regions of uncertainty are a simplification, whereas in reality these regions are continuous probability distributions.

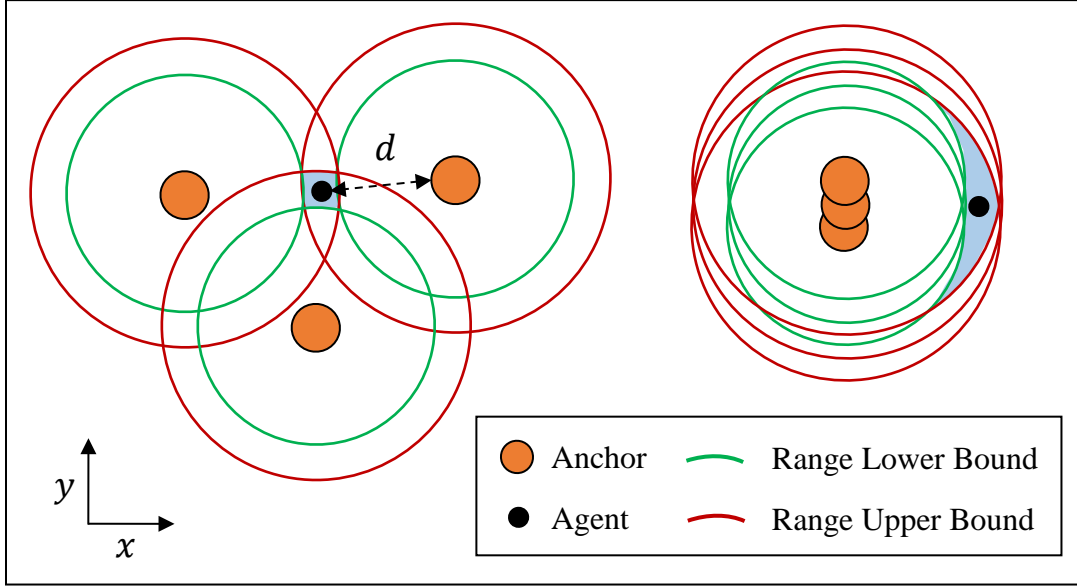


Fig. 2 Example of geometry with low DOP (left) and high DOP (right)

## 2.2 GPS DOP

More formally, DOP measures the degree to which range measurement errors affect the accuracy of the agent's position. Using the Jacobian matrix  $\mathbf{J}$  from Eq. 10, the  $\mathbf{Q} \in \mathbb{R}^{4 \times 4}$  matrix is formulated as

$$\mathbf{Q} = (\mathbf{J}^T \mathbf{J})^{-1}. \quad (11)$$

The diagonal elements of  $\mathbf{Q}$  are the variances of  $x_i$

$$Q_{ii} = \sigma_{x_i}^2. \quad (12)$$

For GPS, DOP values are expressed as<sup>7</sup>

- Horizontal DOP (HDOP)
- Vertical DOP (VDOP)
- Position DOP (PDOP)
- Time DOP (TDOP)
- Geometric DOP (GDOP)

Using  $x$ ,  $y$ ,  $z$ , and  $t$  for the elements of  $\mathbf{x}$ , these DOP values are

$$HDOP = \sqrt{\sigma_x^2 + \sigma_y^2}, \quad (13)$$

$$VDOP = \sqrt{\sigma_z^2}, \quad (14)$$

$$PDOP = \sqrt{\sigma_x^2 + \sigma_y^2 + \sigma_z^2}, \quad (15)$$

$$TDOP = \sqrt{\sigma_t^2}, \quad (16)$$

and

$$GDOP = \sqrt{\sigma_x^2 + \sigma_y^2 + \sigma_z^2 + \sigma_t^2}. \quad (17)$$

For completeness, 2 more DOP values are defined here as

$$XDOP = \sqrt{\sigma_x^2}, \quad (18)$$

and

$$YDOP = \sqrt{\sigma_y^2}. \quad (19)$$

For consistency, VDOP will also be referred to here as ZDOP.

Figure 3 shows 2 examples of swarm geometries. Each anchor is a red circle positioned at the vertex of a cube. On the left, the agent is positioned in the center of the cube surrounded by the anchors, creating a symmetric geometry with the low DOP values listed in Table 1. On the right, the agent is moved away from the anchors, creating a condensed grouping of anchors from the perspective of the agent, resulting in the higher DOP values in Table 1.

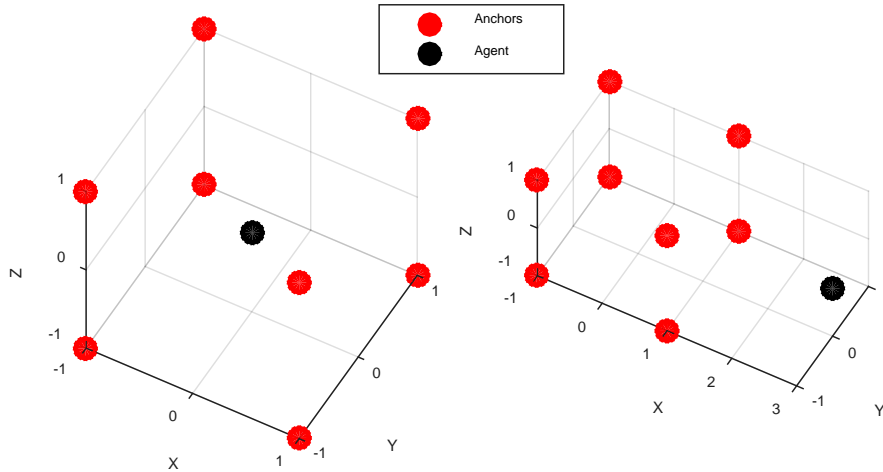


**Fig. 3** An example geometry with a low PDOP (left) and a high PDOP (right)

Table 1 GPS DOP values for Fig. 3

DOP type	Low PDOP example	High PDOP example
XDOP	0.8	4.2
YDOP	0.8	1.3
ZDOP	0.8	1.3
TDOP	0.4	3.2
PDOP	1.4	4.6
GDOP	1.4	5.7

### 2.3 Comparison of GPS DOP to Root-Mean-Square Error

The simulation in Fig. 1 was repeated with  $\sigma = 0.01$ , this time using 100 sets of measurements (with each set containing all agent-to-anchor ranges) for 31 different agent positions. The agent was moved along the  $x$  axis from  $x = 0$  to  $x = 3$ , as illustrated in the geometries in Fig. 3. Plots for 6 of these agent positions are shown in Fig. 4. These results are as expected when compared to typical GPS scenarios. The earth blocks satellites below the horizon, resulting in geometries where all of the anchors are on one side the agent. For GPS, this is in the vertical direction and causes VDOP to be larger than HDOP. This is the reason why GPS DOP values are divided into vertical and horizontal components. In this example all of the anchors are offset in the  $x$  direction, resulting in increasing XDOP as the agent moves farther away from the anchors. Figure 5 plots the GDOP, XDOP, YDOP, ZDOP, and TDOP values scaled by  $\sigma$  and compares them to their respective root-mean-square error (RMSE) values. The DOP values appear to track the RMSE well.

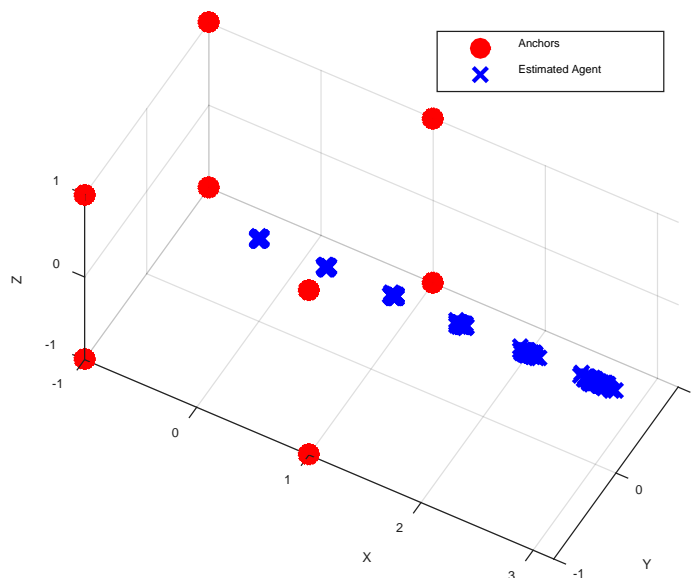


Fig. 4 Agent location estimation from noisy TOF range measurements for 6 different agent locations

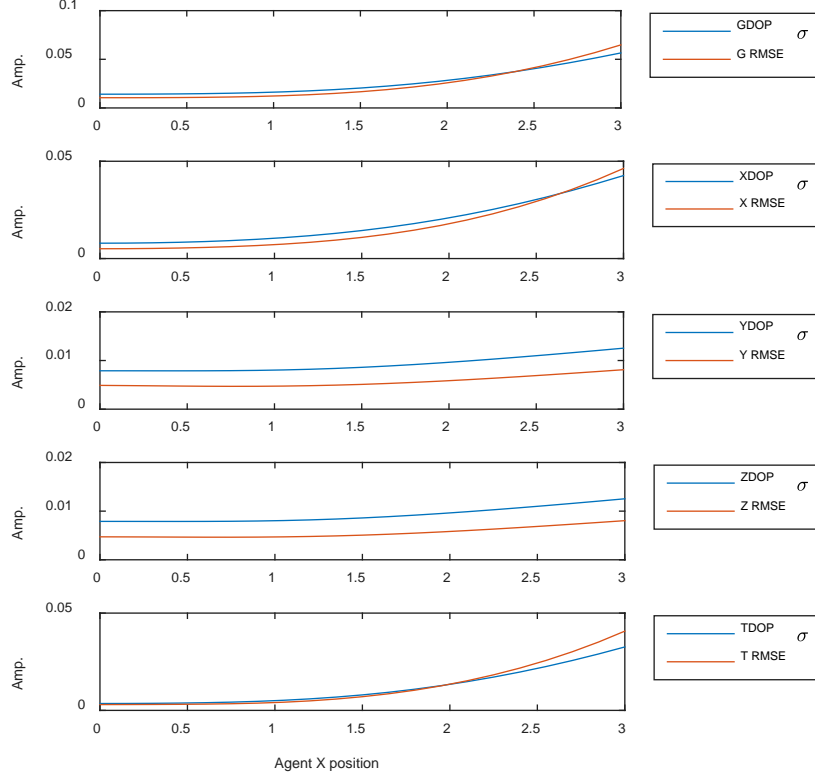


Fig. 5 Comparison of DOP and RMSE values for the simulation in Fig. 4

### 3. TWR Localization and DOP with Anchors

#### 3.1 TWR Localization and DOP Derivation

GPS uses TOF ranging, which requires expensive infrastructure to synchronize the clocks on the GPS satellites. This one-way TOF ranging is necessary for GPS because of the large distances between the agent and the satellites. In the case of smaller geometries, like those typically used for swarm localization, TWR can be used to range between anchors and agents. This method is independent of time synchronization, which reduces system requirements. Excluding a clock-based offset from the equations, the pseudorange for agent  $i$  becomes distance  $d_i$ . The Gauss–Newton residuals are now

$$r_i = \|\mathbf{a}_i - \mathbf{x}\| - d_i, \quad (20)$$

where  $\mathbf{x} \in \mathbb{R}^3$  is the estimated position of the agent. The residuals are the differences between the estimated distances to the agent and measured distances. As before, the position  $\mathbf{x}$  is found by minimizing the sum of squares of the residuals using the Jacobian matrix, which is now  $\mathbf{J} \in \mathbb{R}^{n \times 3}$ , to iteratively solve for  $\mathbf{x}$ . The

derivation of  $J$  proceeds as before without the elements representing the clock offset.

$$J_{ij} = \frac{\partial r_i(\mathbf{x})}{\partial x_j} = \frac{x_j - \mathbf{a}_{ij}}{\|\mathbf{a}_i - \mathbf{x}\|}. \quad (21)$$

Once again, the  $Q \in \mathbb{R}^{3 \times 3}$  matrix is formulated as

$$Q = (J^T J)^{-1} \quad (22)$$

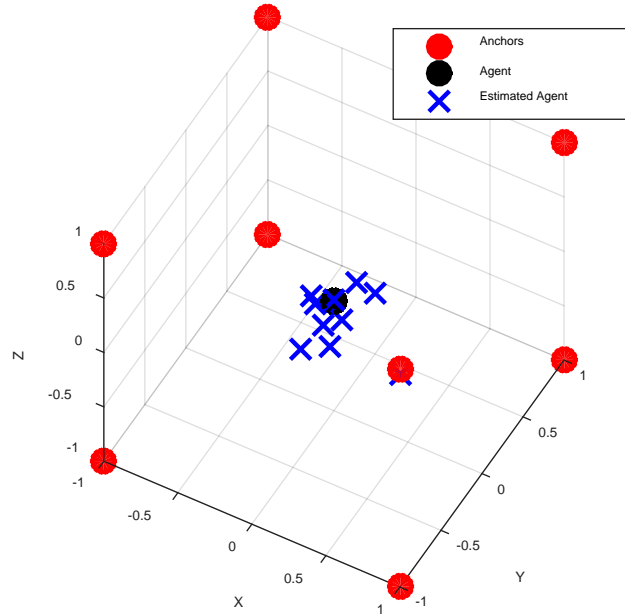
and used to calculate the DOP values. Since there is no time dilution, TDOP and GDOP values are no longer defined. Using the example geometries in Fig. 3, Table 2 shows the new DOP values for the case of TWR. Removing the clock offset has greatly decreased the DOP and has also changed the relative magnitudes of the DOP components. In the GPS example, the XDOP value was the largest and resulted in the most RMSE. Here, the XDOP actually decreases and the YDOP and ZDOP increase. These results are understandable when we consider that the TWR DOP is comparable to the intuitive example in Fig. 2, where the YDOP increased when the agent was placed far away from the anchors along the  $x$  axis. In the case of GPS, the increase in XDOP can now be seen to have been a result of the time dilution.

**Table 2** TWR DOP values for Fig. 3

DOP type	Low PDOP example	High PDOP example
<b>XDOP</b>	0.6	0.4
<b>YDOP</b>	0.6	1.1
<b>ZDOP</b>	0.6	1.1
<b>PDOP</b>	1.1	1.6

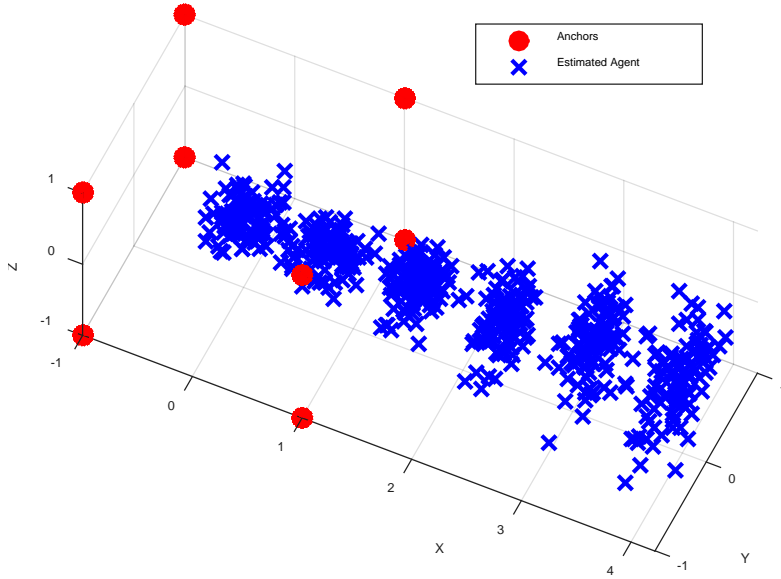
### 3.2 Comparison of TWR DOP and RMSE Using Anchors

Figure 6 shows the geometry used previously with anchors positioned on the vertices of a unit cube and the agent at the center. Ten sets of range measurements were simulated using the modified Gauss–Newton algorithm for TWR with unbiased Gaussian noise and standard deviation  $\sigma = 0.25$ , resulting in 10 estimated agent positions marked by blue “X’s”.



**Fig. 6 Agent location estimation from noisy TWR measurements using Gauss–Newton algorithm**

The simulation in Fig. 6 was repeated with  $\sigma = 0.01$ , using 100 sets of measurements (with each set containing all agent-to-anchor ranges) for 31 different agent positions. The agent was moved along the  $x$  axis from  $x = 0$  to  $x = 4$ , similar to the geometries in Fig. 3. The results are shown in Fig. 7 with the greater YDOP and ZDOP values evident from the spreading of the estimated locations in the  $yz$ -plane. Figure 8 shows a comparison between the DOP values scaled by  $\sigma$  and the RMSE. The top plot compares the scaled PDOP to the total RMSE, denoted P RMSE. The other plots compare the separate  $x$ ,  $y$ , and  $z$  RMSE to their respective scale DOP values. Once again, the DOP values appear to track the RMSE well.



**Fig. 7** Agent location estimation from noisy TWR measurements for 6 agent locations

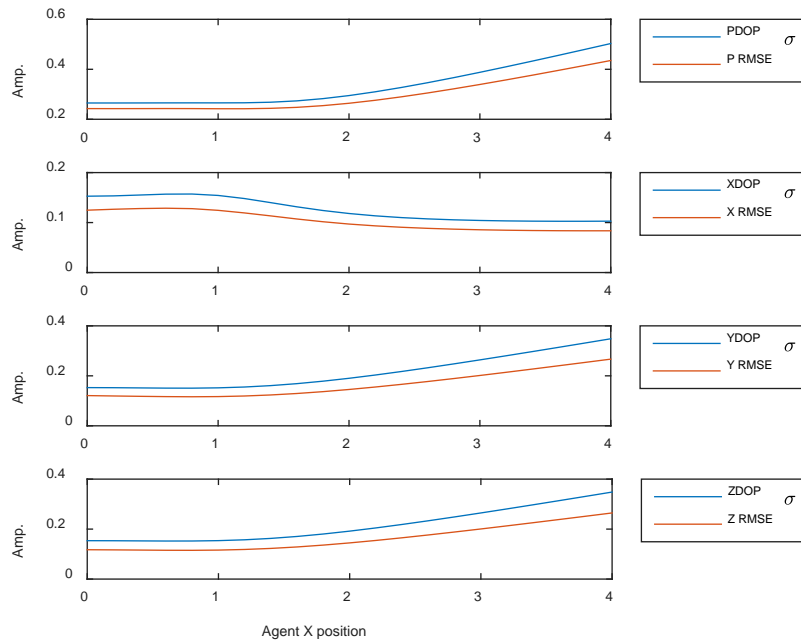


**Fig. 8** Comparison of DOP and RMSE values for the simulation in Fig. 7

## 4. Swarm Relative Localization and DOP

---

### 4.1 Swarm Relative Localization

---

In the case of a swarm of agents, none of the agent positions are known, requiring a different algorithm to solve for the relative localization of the agents. One such algorithm is classical multidimensional scaling (MDS)<sup>11</sup>, which proceeds as follows. Let  $\mathbf{D}^{\odot 2} \in \mathbb{R}^{n \times n}$  be the squared Euclidean distance matrix composed of elements  $d_{ij}^2$  representing the squared distance from agent  $i$  to agent  $j$ .  $(\cdot)^{\odot 2}$  denotes the Hadamard (element-wise) exponentiation.  $\mathbf{D}^{\odot 2}$  is double-centered by

$$\mathbf{B} = -\frac{1}{2}\mathbf{C}\mathbf{D}^{\odot 2}\mathbf{C}, \quad (23)$$

where  $\mathbf{C}$  is the centering matrix

$$\mathbf{C} = \mathbf{I} - \frac{1}{n}\mathbb{O}. \quad (24)$$

$\mathbf{I} \in \mathbb{R}^{n \times n}$  is the identity matrix, and  $\mathbb{O} \in \mathbb{R}^{n \times n}$  is a matrix of all 1's. The agent location matrix  $\mathbf{X} \in \mathbb{R}^{n \times 3}$  is then the first 3 columns of  $\mathbf{X}'$  given by

$$\mathbf{X}' = \mathbf{E}\mathbf{\Lambda}^{\odot 1/2}, \quad (25)$$

where  $\mathbf{E}$  is a matrix of the  $n$  eigenvectors of  $\mathbf{B}$ , and  $\mathbf{\Lambda}$  is a diagonal matrix of the corresponding  $n$  eigenvalues of  $\mathbf{B}$  in descending order.

Since only the relative localization is determined, localization calculations may differ in rotation, translational, and reflection. This makes it difficult to calculate RMSE in Monte Carlo simulations. To align swarm positions, they can be rotated, translated, and reflected to minimize the RMSE to a given reference using the Kabsch algorithm.<sup>12</sup> For swarm localization simulations, the true agent positions  $\mathbf{X}_1$  are used as reference for the estimated location matrix  $\mathbf{X}_2$ . The Kabsch algorithm starts by calculating and subtracting the centroids of  $\mathbf{X}_1$  and  $\mathbf{X}_2$  giving

$$\mathbf{P}_1 = \mathbf{X}_1 - \frac{1}{n}\mathbb{O}\mathbf{X}_1 \quad (26)$$

and

$$\mathbf{P}_2 = \mathbf{X}_2 - \frac{1}{n}\mathbb{O}\mathbf{X}_2. \quad (27)$$

Next, the cross covariance matrix is calculated as

$$\mathbf{A} = \frac{1}{n} \mathbf{P}_1^T \mathbf{P}_2. \quad (28)$$

Using singular value decomposition,  $\mathbf{A}$  is represented as

$$\mathbf{A} = \mathbf{U} \mathbf{W} \mathbf{V}^T. \quad (29)$$

The rotation matrix is then

$$\mathbf{R} = \mathbf{U} \mathbf{V}^T \quad (30)$$

and the translation is

$$\mathbf{t} = \frac{1}{n} \mathbf{X}_1^T \mathbf{1} - \frac{1}{n} \mathbf{X}_2^T \mathbf{1} \mathbf{R}, \quad (31)$$

where  $\mathbf{1} \in \mathbb{R}^{n \times 1}$  is a vector of all 1's. Typical applications of the Kabsch algorithm ensure  $|\mathbf{R}| \geq 0$  to prevent reflection. Here reflection is allowed to correct for any reflection caused by the classical MDS algorithm.

## 4.2 Comparison of Average TWR DOP to RMSE

---

### 4.2.1 Increasing DOP Example

Using classical MDS and the Kabsch algorithms, a simulation was constructed to test the DOP with respect to swarm relative localization. Figure 9 shows the initial true locations of 8 agents. Thirty-one different swarm configurations were generated from the initial locations by scaling all of the agents'  $x$  coordinates and some of the agents'  $z$  coordinates as shown in Fig. 10. The resulting swarm geometries progressively become wider in the  $x$  and  $z$  directions but remain narrow along the  $y$  axis. (For visualization purposes, the  $y$  axis of the plot is scaled differently than the  $x$  and  $z$  axes.)

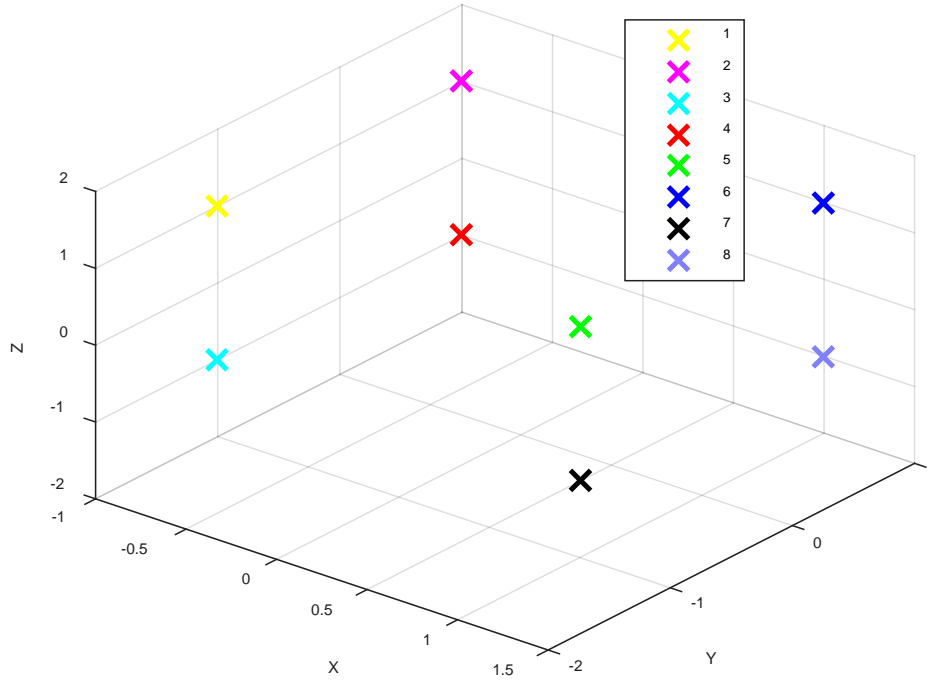


**Fig. 9 Initial agent locations for swarm DOP simulation**

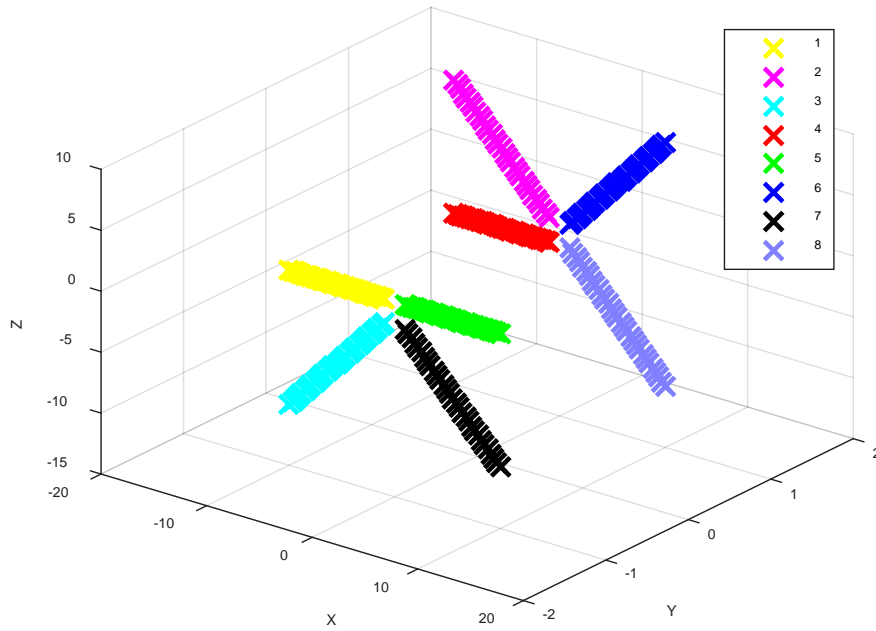


**Fig. 10 Thirty-one different swarm positions generated from Fig. 9 by scaling all of the x coordinates of the agents and some of the z coordinates**

For each of these 31 swarms, 100 sets of Euclidean distance matrices were generated with additive Gaussian noise with standard deviation  $\sigma = 1$ . Classical MDS and the Kabsch algorithms were then used to estimate the agent locations.

Approved for public release; distribution is unlimited.

The results for 6 of these 31 swarm configurations are shown in Fig. 11. Unlike localization with anchors, the positions of all of the agents in the swarm are localized and affected by the swarm geometry. Therefore, to characterize the swarm DOP, the TWR DOP for each agent was calculated relative to the other agents and averaged. Figure 12 shows a comparison between these average DOP values scaled by  $\sigma$  and the average RMSE. The top plot compares the scaled PDOP to the total RMSE. The other plots compare the separate  $x$ ,  $y$ , and  $z$  RMSE to their respective scale DOP values. The scaling of the  $x$  and  $z$  components of the agent positions creates diversity on those planes, which keeps the XDOP and ZDOP low. The  $y$  components remain the same, effectively decreasing the diversity along the  $y$  planes compared to the  $x$  and  $z$  planes, increasing the YDOP. The RMSE values follow the trend of the DOP values, with the XDOP and ZDOP staying flat and the YDOP increasing. The  $y$  RMSE rises at a slower rate than the YDOP, however. The fact that the RMSE values here do not track the DOP values as well as the anchor case is not surprising. The relationships here are more complex since we are solving for the positions of all of the agents. In addition, we are using average YDOP and RMSE values, which further complicates DOP calculations.

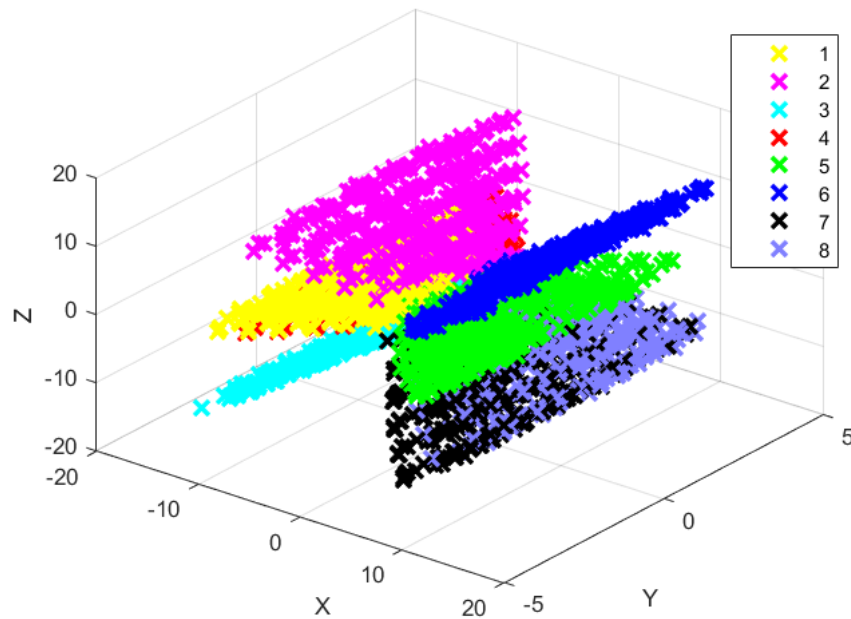


**Fig. 11** Estimated swarm position from noisy measurements for 6 of the swarms shown in Fig. 10

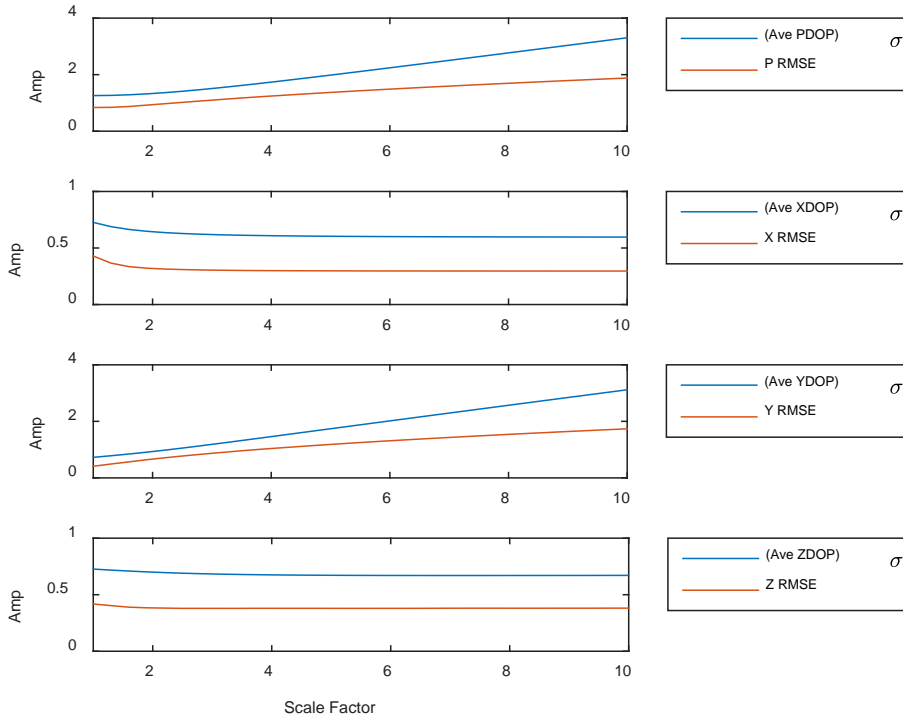


**Fig. 12 RMSE error and average DOP results for the simulation in Fig. 11**

#### 4.2.2 Constant DOP Example

Compare the results of the previous simulation to those shown in Figs. 13 and 14. Instead of only scaling the separate  $x$  and  $z$  components of the agent's positions, all of the components were scaled. This retained the same geometry and hence the same DOP values as the scale factor was increased. Whereas Fig. 11 shows the  $y$  RMSE increasing with the scale factor, Fig. 13 shows the RMSE remaining constant like the DOP values. Figure 14 confirms the observations from Fig. 13, with the DOP and RMSE remaining flat as the scale factor is increased. Thus, we see that the average TWR DOP performs as expected, remaining the same across similar swarm geometries.

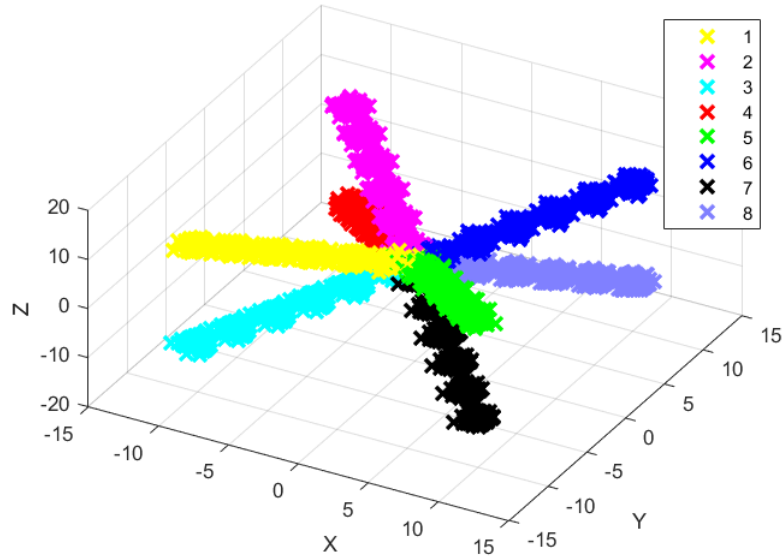


**Fig. 13** Estimated swarm position from noisy measurements for 6 swarms with all components of the agent's positions linearly scaled

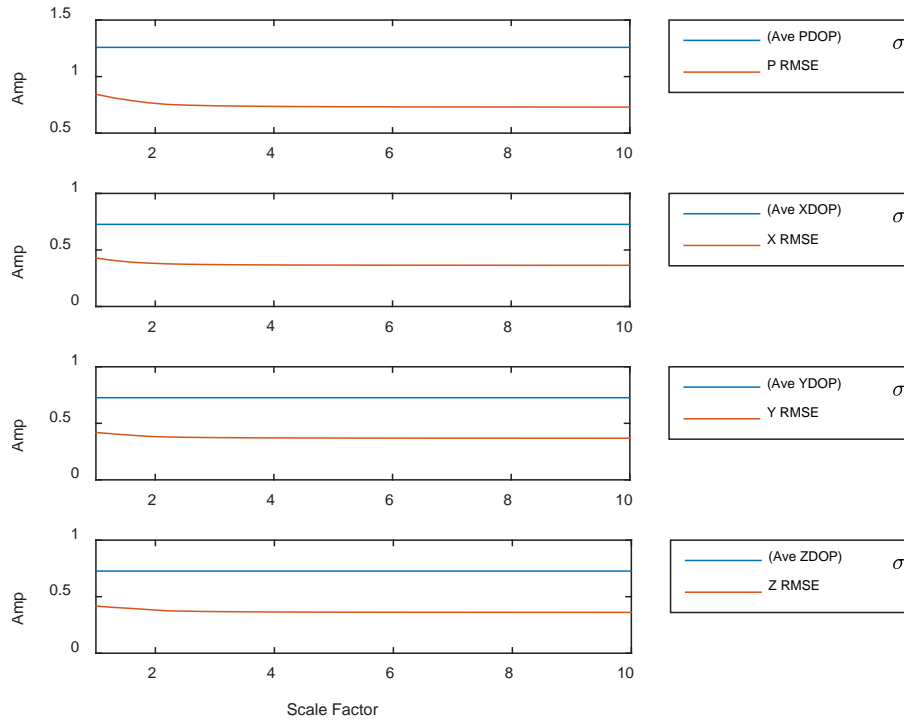


**Fig. 14** RMSE error and average DOP results for the simulation in Fig. 13

### 4.2.3 Example of Inconsistent DOP and RMSE Values

The RMSE does not always track average DOP values as well as demonstrated so far. Figures 15 and 16 show a case where only one agent's position is scaled in the  $x$  direction. We would expect that just as the YDOP and ZDOP should increase, so too the  $y$  and  $z$  RMSE should increase. Instead, the  $y$  and  $z$  RMSE actually slightly decreases.

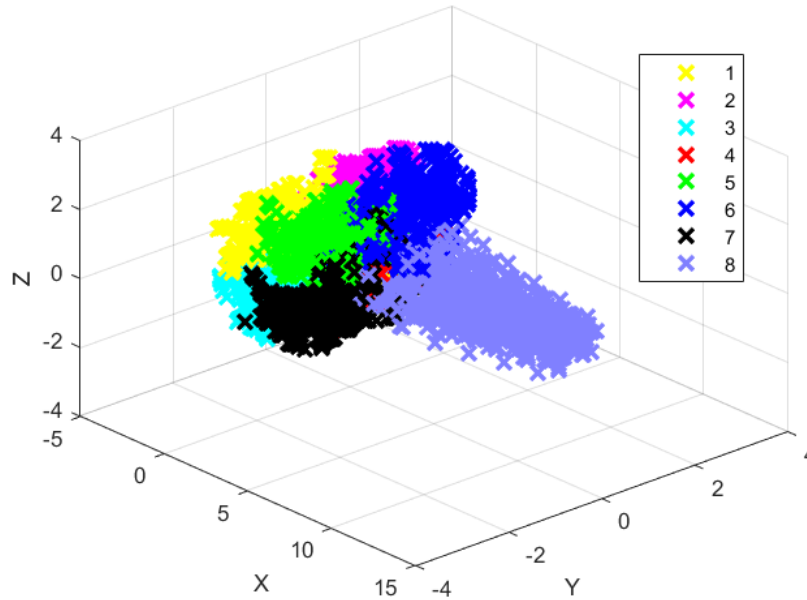


**Fig. 15** Estimated swarm position from noisy measurements for 6 swarms with only one agent's position scaled

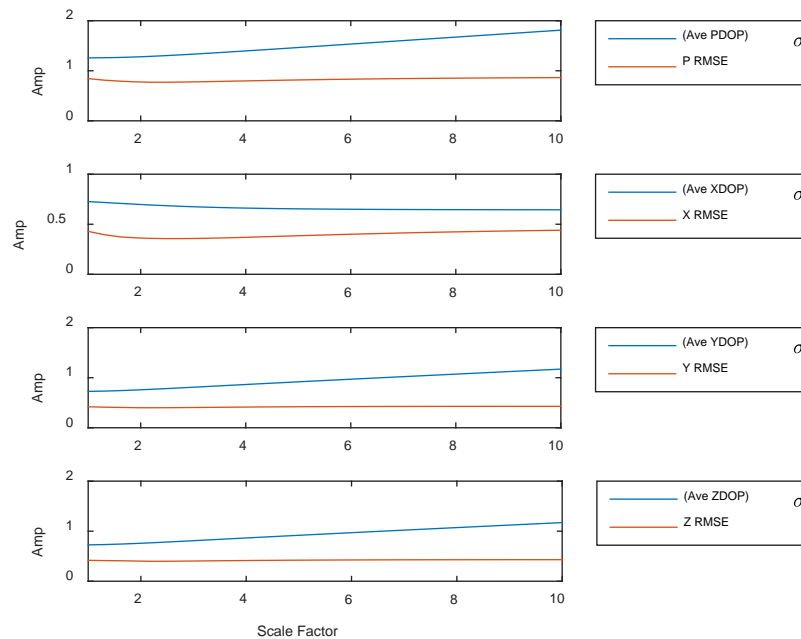


**Fig. 16** RMSE error and average DOP results for the simulation in Fig. 15

A possible explanation for this phenomenon is that the  $y$  and  $z$  RMSE of the scaled agent does actually increase, and the observed decrease is caused by using the Kabsch algorithm to align the simulation results. To test this theory, the same swarm geometries were used, except noise was added directly to the position of the scaled agent. No range measurements were made, and classical MDS was not used. Only the Kabsch algorithm was employed to align the simulation sets. Figure 17 shows the results of a set of 100 simulations for the scaled agent at its original position. Figure 18 shows the simulations for a scale factor of 10, and Fig. 19 compares the RMSE of the scaled agent to the average of the other agents. Once again, the RSME decreases as the agent's position is scaled, even though the same amount of noise was directly added to the agent's position in every simulation. We can also see error in the other agents, even though no noise was added to their positions. Clearly the culprit of the decreasing error is the Kabsch algorithm. The Kabsch algorithm rotates the swarm to decrease the total error, effectively adding noise to the other agents. As the scale factor is increased and the scaled agent moves farther out from the swarm center, less rotation is necessary to adjust the scaled agent's position, leading to a decrease in error for all of the agents. This does not eliminate the error caused by the growing DOP, it only means that in this instance the ability of the Kabsch algorithm to correct for relative localization error grows faster than the error caused by the DOP.

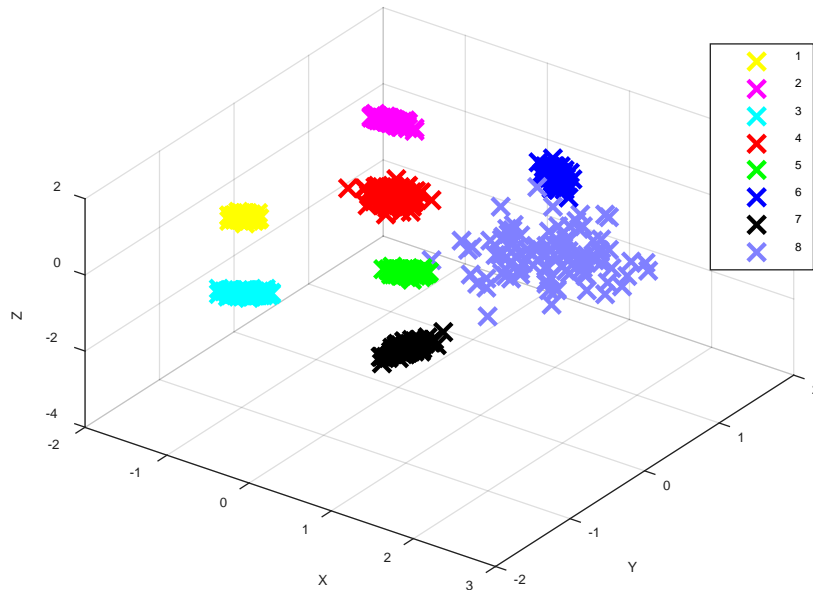


**Fig. 17 Results of Kabsch algorithm after noise was added directly to the position of agent 8, with the scale factor set to 1**

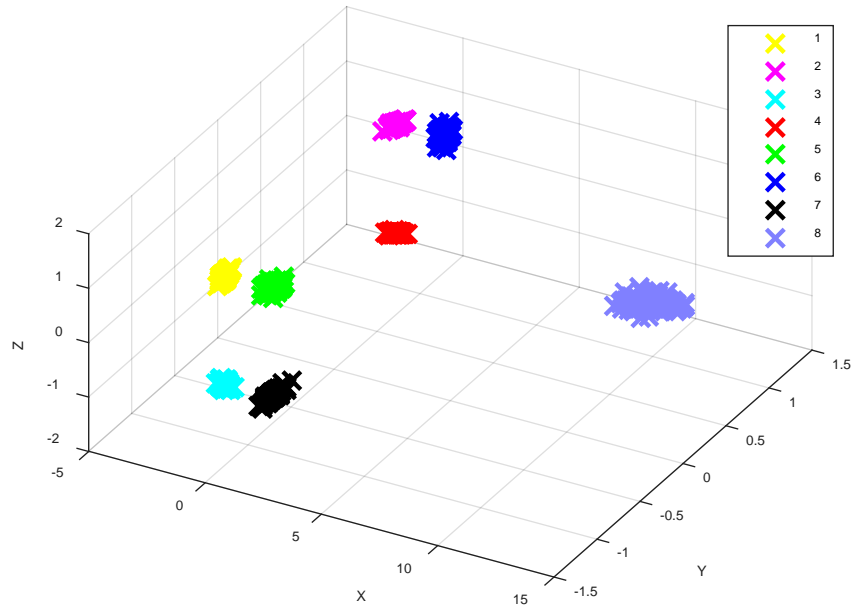


**Fig. 18** Results of Kabsch algorithm after noise was added directly to the position of agent 8, with the scale factor set to 10

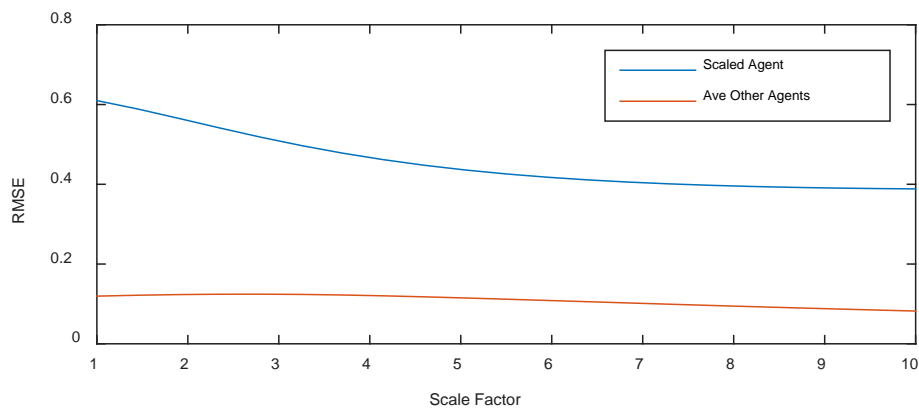


**Fig. 19** A comparison of the RMSE of the scaled agent to the average of the other agents

### 4.3 A Simple Application for Swarm Relative Localization DOP

A simple application for DOP in swarm system design is the determination of the swarm size. Intuitively, the greater the number of swarm agents, the lower the DOP, and the lower the resulting position RMSE. As a test case, 4 platonic solids were chosen that should have optimal DOP values because of their symmetric geometry. One hundred simulations were run for each case with unbiased Gaussian noise with standard deviation  $\sigma = 0.5$  added to the range measurements. Table 3 summarizes the results, listing the average TWR PDOP and RMSE for all of the agents. The estimated agent positions for the 3 cases are also shown in Fig. 20. As expected,

the RMSE decreases with the PDOP. Although many factors may influence swarm system design, DOP can be a useful tool in balancing cost versus the benefit of lower localization error due to swarm size.

**Table 3 PDOP and RMSE values for different swarm sizes**

Swarm geometry	$n$ agents	PDOP	RMSE
Octahedron	6	1.53	0.42
Cube	8	1.26	0.38
Icosahedron	12	0.98	0.34
Dodecahedron	20	0.74	0.28

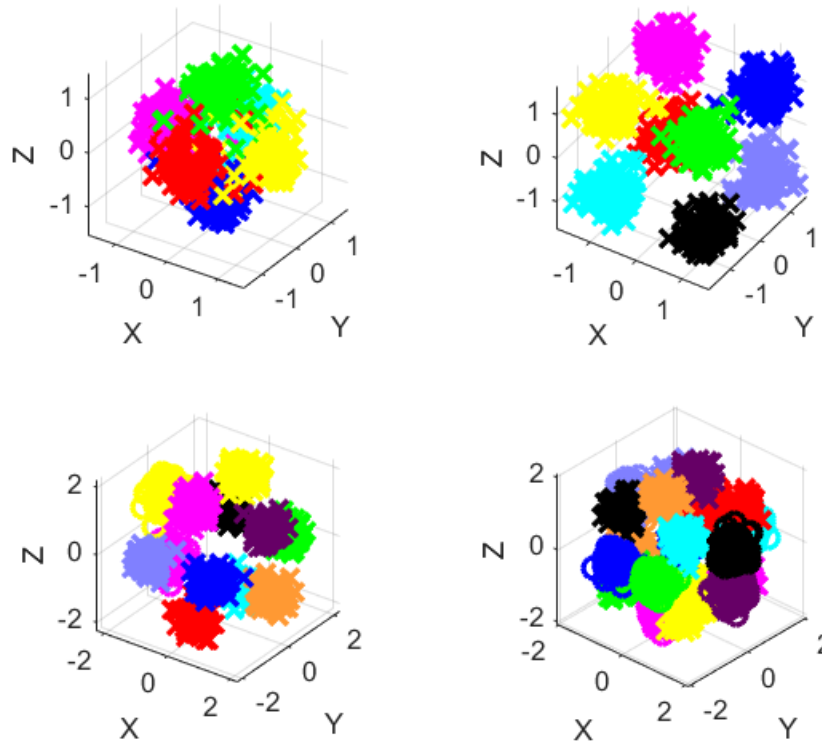


**Fig. 20** Four cases of swarm relative localization with different swarm sizes. The upper left has 6 agents, the upper right 8, lower left 12, and the lower right 20 agents.

## 5. Conclusion

DOP is an important parameter in localization and must be taken into account during system design to predict and limit estimated position errors. Starting with GPS as an example of TOF localization with anchors, a DOP metric for TWR localization with anchors was derived that showed high correlation to RMSE simulations. To apply the TWR DOP to swarm relative localization, average TWR

DOP values were used that incorporated the DOP calculations of all of the agents. This metric correlated well to RMSE simulations in a general case of increasing DOP and in a case where the DOP geometry remained constant but showed inconsistencies in a case where only one agent was moved away from the rest of the swarm. This inconsistency was shown to be a result of the Kabsch transformation, however, and did not invalidate the average TWR DOP metric. Finally, a simple application of DOP for swarm design was demonstrated.

Now that a DOP metric has been proposed for swarm relative localization, it can be applied in future research involving swarm design and modeling. Some research questions include the following:

- What applications exist where the swarm geometry should be optimized to minimize localization error?
- Does the cost of optimizing swarm geometry outweigh other geometry priorities and other ways to reduce localization error?
- How accurately can this DOP metric predict localization error in common swarming applications?
- Can the metric be adjusted to include other localization technologies, such as systems that use angle-of-arrive technologies?

In addition, further research to improve this DOP metric should be explored. The Cramer–Rao bound has been used to set limits on geometry-related error and deserves investigation.<sup>13</sup> In addition, a least-squares formulation for relative localization may directly lead to an improved DOP model. Further research will help to answer these questions and may lead to improvements on this DOP metric for swarm relative localization.

## 6. References

---

1. Kurazume R, Nagata S, Hirose S. Cooperative positioning with multiple robots. In: 1994 IEEE International Conference on Robotics and Automation; 1994 May 8–13; San Diego, CA. p. 1250–1257.
2. Bachrach A, Prentice S, He R, Roy N. RANGE—robust autonomous navigation in GPS-denied environments. *J Field Robot.* 2011;28(5):644–666.
3. Ko Young-Bae, Vaidyia Nitin H. Location-aided routing (LAR) in mobile ad hoc networks. *Wirel Netw.* 2000;6(4):307–321.
4. Parker R, Valae S. Vehicular node localization using received-signal-strength indicator. *IEEE T Veh Technol.* 2007;56(6):3371.
5. Ryan A, Zennaro M, Howell A, Sengupta R, Hedrick JK. An overview of emerging results in cooperative UAV control. 43rd IEEE Conference on Decision and Control; 2004 Dec 14–17; Nassau, Bahamas.
6. Fresconi F, Fermen-Coker M. Delivery of modular lethality via a parent-child concept. In: AIAA Atmospheric Flight Mechanics Conference 2015. 2015 Jan 5–9; Kissimmee, FL. p. 2708.
7. Langley RB. Dilution of precision. *GPS World.* 1999:52–59.
8. Iliev N, Paprotny I. Review and comparison of spatial localization methods for low-power wireless sensor networks. *IEEE Sens J.* 2015;15(10): 5971–5987.
9. Misra P, Burke BP, Pratt MM. GPS performance in navigation. *Proc IEEE.* 1999;87(1):65–85.
10. Björck Å. Numerical methods for least squares problems. Philadelphia (PA): Society for Industrial and Applied Mathematics; 1996.
11. Wickelmaier F. An introduction to MDS. Aalborg University (Denmark): Sound Quality Research Unit; 2003.
12. Kabsch W. A solution for the best rotation to relate two sets of vectors. *Acta Crystallographica Section A.* 1976;32:922–923.
13. Ouyang RW, Wong AKS, Lea CT. Received signal strength-based wireless localization via semidefinite programming: Noncooperative and Cooperative Schemes. *IEEE T Veh Technol.* 2010;59:1307–1318.

## List of Symbols, Abbreviations, and Acronyms

---

DOP	dilution of precision
GDOP	geometric DOP
GPS	global positioning system
HDOP	horizontal DOP
MDS	multidimensional scaling
PDOP	position DOP
RMSE	root-mean-square error
TDOP	time DOP
TOF	time of flight
TWR	two-way ranging
VDOP	vertical DOP

1 DEFENSE TECHNICAL  
(PDF) INFORMATION CTR  
DTIC OCA

2 DIR ARL  
(PDF) IMAL HRA  
RECORDS MGMT  
RDRL DCL  
TECH LIB

1 GOVT PRINTG OFC  
(PDF) A MALHOTRA

26 ARL  
(PDF) RDRL WML F  
B ALLIK  
B J ACKER  
T G BROWN  
S BUGGS  
E BUKOWSKI  
J COLLINS  
J CONDON  
B DAVIS  
M DON  
D EVERSON  
D GRZYBOWSKI  
R HALL  
J HALLAMEYER  
M HAMAOU  
T HARKINS  
M ILG  
B KLINE  
J MALEY  
C MILLER  
P MULLER  
B NELSON  
D PETRICK  
K PUGH  
N SCHOMER  
B TOPPER  
RDRL WML E  
F FRESCONI

INTENTIONALLY LEFT BLANK.